Cite This: J. Phys. Chem. Lett. 2019, 10, 566–573

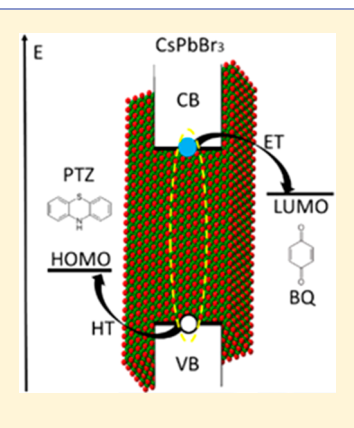
Ultrafast Charge Separation in Two-Dimensional CsPbBr₃ Perovskite **Nanoplatelets**

Qiuyang Li[®] and Tianquan Lian*®

Department of Chemistry, Emory University, 1515 Dickey Drive, NE, Atlanta, Georgia 30322, United States

Supporting Information

ABSTRACT: Two-dimensional (2D) cesium lead halide perovskite colloidal nanoplatelets show sharper excitonic absorption/emission peaks and larger absorption cross section in comparison to bulk materials and quantum dots. It remains unclear how 2D exciton and charge separation properties can be utilized to further enhance the performance of perovskite materials for optoelectrical applications. Herein, we report a study of exciton and interfacial charge-transfer dynamics of CsPbBr₃ nanoplatelets via transient absorption spectroscopy. The exciton binding energy ($\sim 260 \text{ meV}$) is determined via detailed spectral analysis. The exciton bleach is caused by band-edge exciton state-filling with negligible single carrier (electron or hole) contributions. Efficient charge separation can be achieved by selective electron and hole transfers to adsorbed molecular acceptors (benzoquinone and phenothiazine, respectively), and the half-life of the charge-separated state (>100 ns) in nanoplatelet-phenothiazine complexes is >100 fold longer than that in quantum dot-phenothiazine complexes. Our results suggest that CsPbBr₃ nanoplatelets are promising materials for photocatalysis and photovoltaic applications.



perovskite semiconductors, including hybrid (MAPbX₃, where MA = methylammonium, X = Cl, Br, I) and allinorganic (CsPbX₃, X = Cl, Br, I) perovskites, are a new class of materials with great potential for optoelectrical applications. 1-4 Their high luminescent quantum yield, long carrier lifetime, and long carrier diffusion length have led to impressive performance for light-emitting diodes, ⁵⁻¹³ lasing, ¹⁴⁻²⁷ and low-cost photovoltaics ²⁸⁻³⁰ (with solar-toelectricity conversion efficiency exceeding 20%^{31–40}). Twodimensional (2D) CsPbX₃ (X = Cl, Br, I) colloidal nanoplatelets (NPLs) were introduced into the perovskite family recently with tunable emission from 2.0 to 3.0 eV. 41-45 These colloidal NPLs can be synthesized in ambient conditions at room temperature, 41,43,44 and their 2D morphology gives rise to unique excitonic features, such as large exciton binding energy, 46 sharp absorption and emission peaks, 41,43,44,47,48 and large absorption coefficient. 49 These properties make perovskite NPLs even more promising materials for photocatalysis and optoelectrical applications. However, the properties of charge separation and recombination in these 2D NPLs, which are the key processes during photocatalytic and photovoltaic reactions, remain unclear. On the one hand, the 2D morphology of NPLs is reported to effectively extend the charge-separated state compared to the 0D and 1D nanostructures⁵⁰ and enhance the solar-to-H₂ conversion efficiency. 50-52 On the other hand, the large exciton binding energy due to dielectric confinement effect in 2D morphology^{46,53} is not favorable for exciton dissociation and charge separation (CS). Moreover, charge separation/ recombination properties are determined by the band-edge 2D exciton behaviors in these NPLs. Therefore, systematic studies on exciton and charge-transfer dynamics in CsPbBr₃ NPLs are

important to both fundamental understanding of 2D excitons in these 2D perovskite materials and rational improvements of their photocatalysis and optoelectrical performance.

Herein, we report a systematic study of exciton and interfacial charge-transfer dynamics of CsPbBr3 colloidal NPLs via transient absorption (TA) spectroscopy. The NPL absorption features before and after excitation were analyzed to reveal the binding energy of excitons (~260 meV). The origin of the band edge exciton bleach (XB) signal was examined. The dissociation of excitons by selective interfacial electron transfer (ET) and hole transfer (HT) from the NPL to adsorbed benzoquinone (BQ) and phenothiazine (PTZ), respectively, was studied as a function of acceptor concentration to reveal the time constants for the charge separation and recombination processes.

Sample Characterization. CsPbBr3 NPLs were synthesized following reported procedures with slight modifications.⁴³ The details of the synthesis are described in the Supporting Information. The transmission electron microscopy (TEM) image of CsPbBr₃ NPLs (Figure 1a) shows rectangular morphology with a lateral size of $(26.7 \pm 6.4) \times (8.1 \pm 1.6)$ nm² (Figure S1). The CsPbBr₃ NPLs dispersed in toluene were used for all measurements in this work. The static absorption (Abs, blue circles in Figure 1b) spectrum of NPLs can be fit according to the well-established model for quantum wells (QWs) and consists of the exciton and continuous band transitions (see Supporting Information, section S4). 46,54-57

Received: December 1, 2018 Accepted: January 14, 2019 Published: January 14, 2019

The Journal of Physical Chemistry Letters

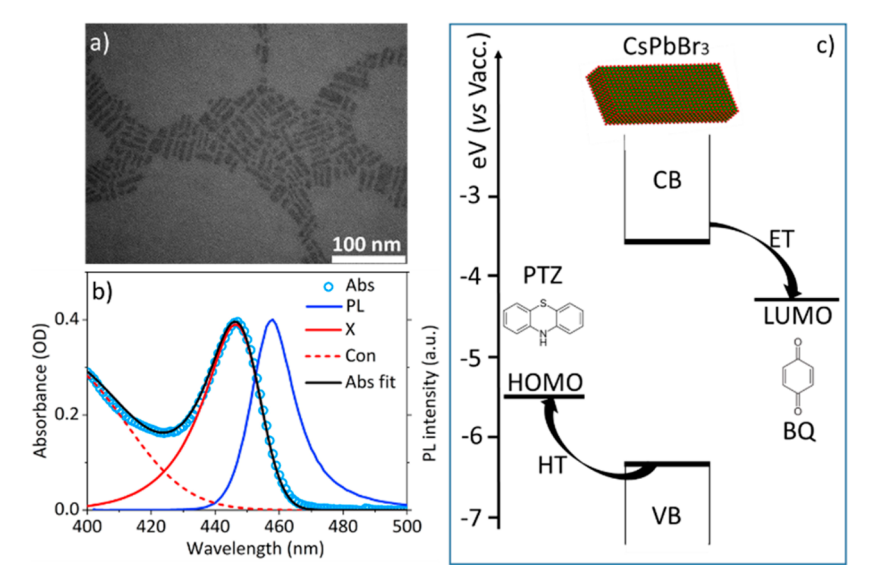


Figure 1. CsPbBr₃ NPLs. (a) TEM image of CsPbBr₃ NPLs. (b) Photoluminescence (solid blue line) and absorption (blue circles) spectra of CsPbBr₃ NPLs. The black solid line is the fit of the absorption spectrum. (c) Scheme of energy levels of CsPbBr₃ NPLs, oxidation potential (HOMO) of PTZ, reduction potential (LUMO) of BQ, and interfacial ET and HT pathways from NPL to molecular acceptors (BQ or PTZ).

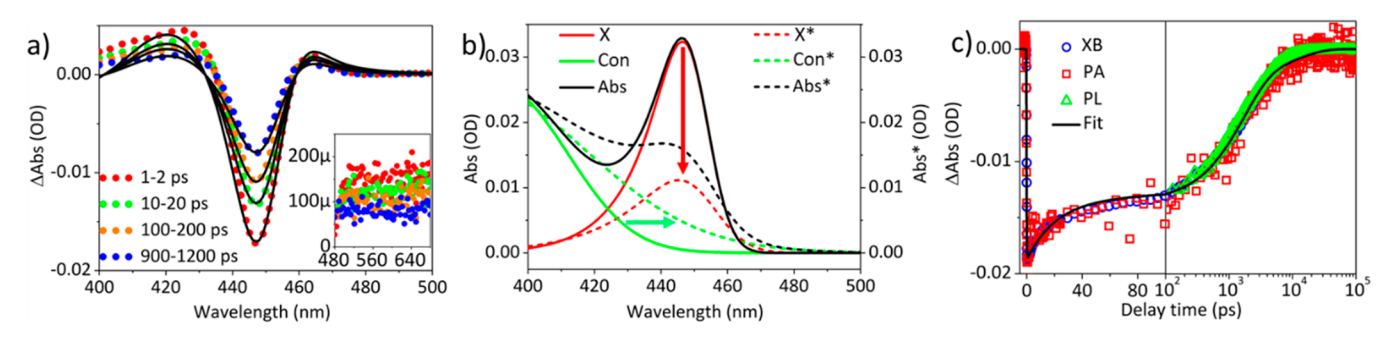


Figure 2. TA spectra and kinetics of free CsPbBr₃ NPLs. (a) TA spectra at indicated delay times (dots) and their fits (solid black lines). Inset: the expanded view of the TA spectra at low-energy range (480–680 nm). (b) Fits of absorption spectra before pump (Abs, solid lines) and after pump (Abs*, dashed lines) that contribute to TA spectra. The arrows show the state-filling (red) and BGR (green) effects on absorption after pump. (c) Comparison of XB, PA, and PL decay kinetics. The solid line is the fit.

The sharp absorption peak at ~2.76 eV (~448 nm) is assigned to the band-edge excitonic transition (X) of 5 monolayer CsPbBr₃ NPLs with a thickness of ~3 nm, ⁴³ and the sharp photoluminescence (PL, blue solid line in Figure 1b) peak at ~2.70 eV (~459 nm) is attributed to band edge emission. 43,46 The full width at half-maximum of the PL peak is 90 ± 2 meV, which is 1.4-fold narrower than CsPbBr₃ QDs (~130 meV),⁵⁸ indicating more uniform quantum confinement along the NPL thickness direction. From the peak position and the onset of the continuous absorption band (Con, from 2.9 to 3.2 eV), the exciton binding energy is determined to be 260 ± 10 meV, which is much larger than that in CsPbBr₃QDs (~40 meV)⁴⁷ and bulk perovskites (~10 meV). 4,59 This binding energy value in CsPbBr3 NPLs is consistent with recently reported $(C_6H_5(CH_2)_2NH_3)_2PbI_4$ nanosheets $(200-260 \text{ meV})^{53}$ but is about 2-fold larger than previously reported CsPbBr₃ NPLs (~120 meV). 46 The band edge positions (vs vacuum) of the conduction band (CB) and valence band (VB) are estimated as -3.59 and -6.34 eV, respectively, which differ from bulk values mainly because of the quantum confinement effect (see Supporting Information, section S3). With the reported reduction potential of BQ at -4.3 eV,⁶⁰ and the reported oxidation potential of PTZ at -5.5 eV,⁶¹ electrons and holes can be selectively transferred from NPLs to BQ and PTZ, respectively (Figure 1c).

Spectroscopy of CsPbBr3 NPLs. We first investigated the exciton dynamics in CsPbBr3 NPLs by TA spectroscopy. All TA measurements in this work were conducted at room temperature with low pump fluence (\sim 5 $\mu J/cm^2$) so that multiexciton generation is negligible and only single exciton dynamics is considered. The TA spectra of free NPLs (Figure 2a) show a negative exciton bleach (XB) signal at ~448 nm, which can be attributed to blocking of the band edge transitions by the presence of a photogenerated band edge exciton. Comparison of normalized TA spectra at all delay times (Figure S3) shows that the spectral shape is independent of delay time from 1 ps to 1.2 ns, consistent with the presence of only long-lived single-exciton states. The spectra also show a broad photoinduced absorption (PA) signal from 480 to 680 nm (inset of Figure 2a), similar to many other low-dimensional semiconductor nanocrystals. 58,61–64 The TA spectra (Figure 2a) can be fit to the difference between the absorption of the excited NPL (Abs*) and ground state (Abs), accounting for exciton-state filling, exciton-exciton interaction, and band gap renormalization (BGR), similar to bulk perovskites⁵⁹ and other 2D NPLs. 55,57 State-filling of continuous band is ignored at the low excitation conditions in which only the single exciton state The Journal of Physical Chemistry Letters

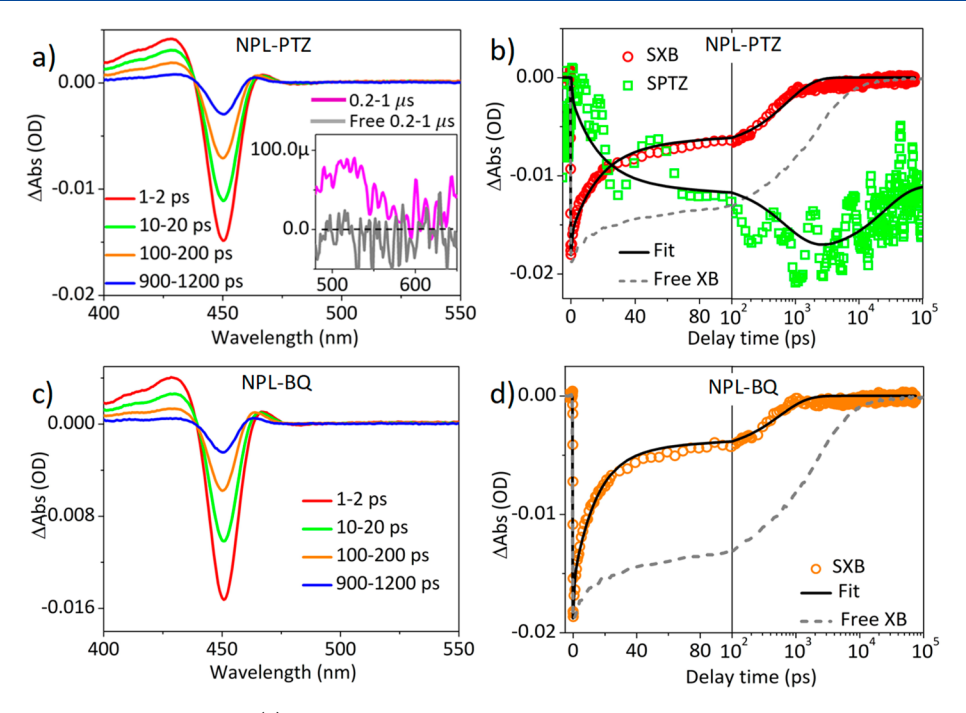


Figure 3. Electron and hole transfer from NPLs. (a) TA spectra of NPL-PTZ complexes at indicated delay times. Inset: a comparison of TA spectra of NPL-PTZ and free NPL at long delay time $(0.2-1~\mu s)$. (b) Comparison of kinetics of subtracted exciton bleach of NPL-PTZ (SXB, red circles), exciton bleach of free NPLs (free XB, gray dashed line), and subtracted oxidized PTZ signals (SPTZ, green squares). The black lines are the fits of SXB and SPTZ kinetics of NPL-PTZ. (c) TA spectra of NPL-BQ complexes at indicated delay times. (d) Comparison of kinetics of subtracted exciton bleach of NPL-BQ (SXB, red circles) and exciton bleach of free NPLs (free XB, gray dashed line). The black lines are the fits of SXB kinetics of NPL-BQ.

is occupied. Abs (solid lines) is obtained by fitting the groundstate spectrum as shown in Figure 1b. Compared to Abs, Abs* (dashed lines, Figure 2b) has a lower exciton peak intensity due to the state-filling of band edge exciton state, broadened peak width, and red-shifted peak position due to excitonexciton interaction.⁵⁷ The continuous feature in the excited NPLs (Con*) is shifted to lower energy because of the BGR^{59,65} (see Supporting Information, section S4 for details). The best fits (black solid lines in Figure 2a) give an exciton shift of 10 ± 2 meV, similar to CsPbBr₃ QDs, ⁴⁸ but smaller than that in CdSe NPLs (~20 meV).⁵⁷ This shift is a net result of exciton–exciton interactions (Δ_{XX}), which contains: (1) red shift due to exciton-exciton Coulomb attraction, also known as the biexciton binding energy 66,67 and (2) blue shift due to Coulomb screening effect, which reduces the exciton binding energy at a higher exciton density.

The XB (~448 nm), PA (500–650 nm), and PL decay kinetics agree with each other (Figure 2c), indicating that both XB and PL probe exciton decay processes. PL decay kinetics before 120 ps is not compared because of the limited instrument response time of the time-resolved PL measurement (~110 ps). The best fit of the XB kinetics gives a formation time of 101 ± 20 fs (see Supporting Information, section S5), indicating fast hot exciton relaxation to the band edge, consistent with recently reported CsPbBr₃ NPLs⁶⁸ and similar to CsPbBr₃ QDs.^{48,58} The decay time constants are 20.8 ± 1.2 ps ($26.8 \pm 2.1\%$), 1664 ± 156 ps ($53.2 \pm 4.4\%$), and 11.4 ± 1.3 ns ($20.0 \pm 4.2\%$) (Table S2), and the half-life of XB kinetics is 804 ± 25 ps, which is faster than the band edge exciton decay reported in CsPbBr₃ QDs (half-life ≈ 2.8 ns).⁵⁸ This may be attributed to enhanced radiative decay rates of band edge excitons in 2D materials^{69–71} and additional

nonradiative pathways in NPLs based on a lower PL quantum yield of NPLs $(\sim 31\%)^{43}$ compared to QDs $(\sim 79\%)$. 54

Charge Separation in CsPbBr3 NPLs. Electron transfer and hole transfer from NPLs were investigated in NPL-BQ and NPL-PTZ complexes, respectively, with varying NPL/ adsorbate ratio by transient absorption spectroscopy. These complexes were prepared by adding different amounts of BQ (PTZ) to NPL toluene solution followed by sonication, and the total BQ (PTZ) concentrations vary from 0.55 (1.12) to 9.25 (7.53) mM. The transient spectra of NPL-PTZ complexes with the highest PTZ concentration (7.53 mM) are shown in Figure 3a. At long delay time (>0.2 μ s), when the TA signal of free NPL decays to zero, a broad peak of NPL-PTZ sample centered at ~525 nm can be seen (inset of Figure 3a), which is attributed to the oxidized PTZ signal.⁶¹ This long-lived oxidized PTZ signal shows that the exciton in NPL dissociates by hole transfer to PTZ to form a charge-separated state with electron remaining in NPL and hole in PTZ. Comparison of XB kinetics of free NPLs and NPL-PTZ shows a faster recovery of the latter in the <1 ns time scale. Interestingly, these samples show the same decay kinetics (Figure S4a) at long delay time (>10 ns), indicating that there exists some free NPLs in the NPL-PTZ sample. The contribution of NPLs with adsorbed PTZ can be represented by the subtracted XB kinetics (SXB), which is obtained by subtracting normalized XB kinetics of free NPL from total XB kinetics of NPL-PTZ (Figure S4a). Because of the overlap between PA and oxidized PTZ signals (Figure S4b), we subtract the normalized PA kinetics (600-650 nm) from the total signal at ~525 nm to obtain the pure oxidized PTX signal, referred to as the subtracted oxidized PTZ kinetics (SPTZ). As shown in Figure 3b, SXB decays faster than XB of free NPLs, consistent with HT from NPL to PTZ. Furthermore, the formation of the

SPTZ signal agrees with the decay of the SXB signal, confirming that the exciton decays by HT from NPL to PTZ. It is important to note that the XB decays to zero at long delay time (>1 ns), when the electron remains in the NPL and the hole is transferred to PTZ, indicating that the VB hole is required for observing an XB signal.

The transient spectra of NPL-BQ complexes with the highest BQ concentration (9.25 mM) are shown in Figure 3c. Similar to the NPL-PTZ sample, the NPL-BQ sample also contains a contribution of free NPLs, whose contribution can be removed by subtracting normalized XB kinetics of free NPL from the XB kinetics of NPL-BQ (Figure S4c). As shown in Figure 3d, the subtracted exciton bleach kinetics (SXB) of NPL-BQ complexes decays faster than the XB of free NPLs (Figure 3d), indicating ET from NPL to BQ. Surprisingly, the SXB of NPL-BQ also decays to zero at a long delay time (>1 ns), indicating a CB electron is also required for the observation of XB.

The results above show that the selective removal of either the CB electron or VB hole results in the complete recovery of XB, which suggest that the band edge exciton transition is blocked by the exciton and that the presence of only the CB electron or VB hole leads to negligible contribution to XB. This is different from either cadmium chalcogenide nanocrystals (QDs,⁷²⁻⁷⁵ NRs,⁷⁶⁻⁷⁸ and NPLs^{64,79-82}), where electron state-filling dominates XB, or CsPbBr₃ QDs, where both electron (\sim 67%) and hole (\sim 33%) state-filling contribute to the XB. 58 Although the origin of this difference is unclear, it is likely due to two properties of CsPbBr₃ NPLs. (1) The effective mass of the electron $(m_e = 0.215m_0)$ is similar to that of the hole ($m_h = 0.211m_0$) in CsPbBr₃ NPLs,⁴³ so that the CB and VB edges likely have similar density of states and phase space-filling behaviors at a thermal equilibrium. (2) The band edge exciton in CsPbBr₃ NPLs is strongly bound (with a binding energy of ~260 meV) so that the exciton wave function is a superposition of many single electron and hole levels. Because the band edge single electron or hole level makes only small contributions to the exciton wave function, neither the CB electron (VB hole) in the charge-separated state, with the electron (hole) in NPL and the transferred hole (electron) in the acceptor, leads to significant exciton bleach.

We fit the XB kinetics of free CsPbBr₃ NPL, SXB kinetics of NPL-BQ/PTZ complexes, and SPTZ kinetics (black solid lines in Figures 2c and 3b,d) using multi-exponential functions with the same set of parameters accounting for band edge recombination, carrier trapping, and CS processes (see Supporting Information, section S5 for details). The best multi-exponential fits give time constants (amplitudes) of 0.55 \pm 0.02 ps (26.8 \pm 2.1%), 17.7 \pm 3.8 ps (53.2 \pm 4.4%), and 724 \pm 84 ps (20.0 \pm 4.2%) for HT and 0.66 \pm 0.03 ps (26.8 \pm 2.1%), 14.7 \pm 2.6 ps (53.2 \pm 4.4%), and 552 \pm 67 ps (20.0 \pm 4.2%) for ET in samples with the highest PTZ (7.53 mM) and BQ (9.25 mM) concentrations, respectively. From these time constants, the HT and ET half-life values can be estimated to be 24.1 \pm 2.5 ps and 10.6 \pm 1.0 ps, respectively. Accounting for the competition between charge separation and recombination, the HT and ET yields are estimated to be 97.6 \pm 0.1% in NPL-PTZ complexes and 97.8 ± 0.1% in NPL-BQ complexes, respectively (see Supporting Information, section S5). The fits also reveal that the charge-separated state in NPL-PTZ is long-lived, whose decay can be fit to a bi-exponential function with time constants (amplitudes) of 31 ± 3 ns (42.8)

 \pm 3.0%) and 4887 \pm 241 ns (57.2 \pm 3.1%) and described by a half-life \gg 100 ns.

Because both the ET and HT times depend on the number of acceptors per NPL, it is useful to quantify these time constants for complexes with one acceptor (BQ or PTZ), referred to as the intrinsic ET and HT time constants. To do this, we analyzed the XB kinetics of NPL-BQ (PTZ) as a function of BO(PTZ) concentrations using a previously reported model for colloidal QDs (see Supporting Information, section S6). 58,83,84 This model assumes (1) the number of acceptors on NPL surfaces follows a Poisson distribution, 85,86 (2) the adsorption of acceptors on NPL surfaces follows the Langmuir adsorption isotherm, 83 and (3) exciton diffusion within 2D NPLs is fast 81,82 and ET and HT rates scale linearly with the number of adsorbed acceptors on the NPL surface.⁵⁸ The apparent exciton quenching rate (the reciprocal of the half-life of XB kinetics, $1/\tau_{1/2}$) as a function of acceptor concentration (Figure S6c) can be fit well according to this model, from which the average number of acceptors per NPL at different acceptor concentrations (Figure S6d) can be obtained. The best fits (solid lines in Figure S6c) yield the intrinsic ET (HT) time constant per BQ (PTZ) of 248 \pm 69 ps (670 \pm 90 ps), which is similar to those in CsPbBr₃ QDs.⁵ This indicates that strong electronic coupling between charge carriers in NPLs and surface adsorbed acceptors results in efficient charge transfer, similar to QDs and nanorods. 62,84,87-91

Compared to CsPbBr₃ QDs, the 2D morphology of CsPbBr₃ NPLs results in the following distinguishing advantages: (1) The strong dielectric confinement effect gives large exciton binding energy so that the exciton rather than free carriers dominates at the band-edge, which increases the oscillator strength of band-edge transitions and is promising for emitting applications. (2) The charge-separated state lifetime of CsPbBr₃ NPL-PTZ complexes (with half-life ≫100 ns) is over 100-fold longer than that in CsPbBr₃ QD-PTZ complexes (with half-life of ~1 ns).⁵⁸ We attribute the longer chargeseparated state lifetime to the 2D morphology, on the basis of our previous findings of 2D CdS NPLs. 50 Although for the same reason we also expect a longer charge-separated state lifetime in NPL-electron acceptor complexes than that in QDelectron acceptor complexes, we are unable to probe the charge-separated state in NPL-BQ complexes because the reduced form of BQ does not have an absorption feature in the visible region (400-800 nm). Considering charge recombination is the main loss pathway for solar-to-fuel conversion, 50 the longer-lived charge-separated state in CsPbBr₃ NPL-acceptor complexes shows greater potential than perovskite QDs for photocatalysis. (3) NPLs have larger absorption coefficient, ⁴⁹ making NPLs potentially better sensitizers in photovoltaics. Therefore, with near unity CS yield, high CS rate, long CS distance, and large absorption cross section, CsPbBr3 NPLs are promising as a novel class of photocatalysis and optoelectrical materials. 45,92,93

In summary, we have studied the exciton dynamics and charge-transfer processes in CsPbBr₃ NPLs via TA spectroscopy. The exciton binding energy (~260 meV) is determined via detailed analysis on static and transient absorption spectra. The XB of CsPbBr₃ NPLs requires exciton at band edge, and single carriers (electron or hole) have negligible contributions to the XB, which is different from either CsPbBr₃ QDs or low-dimensional cadmium chalcogenide nanocrystals. ET and HT from NPLs to electron (BQ) and hole (PTZ) acceptors,

respectively, were observed, and their rates increase at higher acceptor contractions. The ET and HT time constants are determined to be 248 \pm 69 and 670 \pm 90 ps per BQ and PTZ, respectively, and reach 24.1 ± 2.5 and 10.6 ± 1.0 ps, respectively, at the highest PTZ (7.53 mM) and BQ (9.25 mM) concentrations studied in our work. At these concentrations, the HT and ET yields are estimated to be $97.6 \pm 0.1\%$ in NPL-PTZ complexes and $97.8 \pm 0.1\%$ in NPL-BQ complexes and the half-life time of the charge-separated state in NPL-PTZ complexes exceeds 100 ns, which is over 100-fold longer than that in CsPbBr₃ QD-PTZ complexes. The findings in this work enhance fundamental understanding of exciton properties and carrier dynamics in 2D perovskite nanomaterials. Moreover, the observations of ultrafast interfacial charge transfer and long-lived charge-separated state of NPL-acceptor complexes suggest they are also promising materials for photocatalysis and solar cell applications.

EXPERIMENTAL METHODS

Sample Synthesis. The colloidal CsPbBr₃ NPLs were synthesized following the reported procedures with slight modifications. ⁴³ Details can be found in the Supporting Information, section S1.

Experimental Setup. Instrumental information describing optical characterization of NPLs are provided in detail in the Supporting Information, section S2. Femtosecond transient absorption (TA) measurements were based on a regeneratively amplified Ti:sapphire laser system (Coherent Legend, 800 nm, 150 fs, 2.4 mJ/pulse, and 1 kHz repetition rate). The TA signals were collected and analyzed by the Helios (femtosecond scale) and the EOS (nanosecond scale) spectrometer (Ultrafast Systems LLC). PL measurements were performed with a FluoroMax-3 Spectrofluorometer (Horiba Scientific).

ASSOCIATED CONTENT

S Supporting Information

The Supporting Information is available free of charge on the ACS Publications website at DOI: 10.1021/acs.jp-clett.8b03610.

Synthesis procedure, additional transient absorption spectra and kinetics, fitting procedures, and fitting parameters (PDF)

AUTHOR INFORMATION

Corresponding Author

*E-mail: tlian@emory.edu.

ORCID @

Qiuyang Li: 0000-0002-8192-3960 Tianquan Lian: 0000-0002-8351-3690

Notes

The authors declare no competing financial interest.

ACKNOWLEDGMENTS

This work is funded by a grant from the National Science Foundation (CHE-1709182).

REFERENCES

(1) Stranks, S. D.; Snaith, H. J. Metal-Halide Perovskites for Photovoltaic and Light-Emitting Devices. *Nat. Nanotechnol.* **2015**, *10*, 391–402.

- (2) Sutherland, B. R.; Sargent, E. H. Perovskite Photonic Sources. *Nat. Photonics* **2016**, *10*, 295–302.
- (3) Zhao, Y.; Zhu, K. Organic-Inorganic Hybrid Lead Halide Perovskites for Optoelectronic and Electronic Applications. *Chem. Soc. Rev.* **2016**, 45, 655–689.
- (4) Manser, J. S.; Christians, J. A.; Kamat, P. V. Intriguing Optoelectronic Properties of Metal Halide Perovskites. *Chem. Rev.* **2016**, *116*, 12956–13008.
- (5) Tan, Z. K.; Moghaddam, R. S.; Lai, M. L.; Docampo, P.; Higler, R.; Deschler, F.; Price, M.; Sadhanala, A.; Pazos, L. M.; Credgington, D.; Hanusch, F.; Bein, T.; Snaith, H. J.; Friend, R. H. Bright Light-Emitting Diodes Based on Organometal Halide Perovskite. *Nat. Nanotechnol.* **2014**, *9*, 687–692.
- (6) Cho, H. C.; Jeong, S. H.; Park, M. H.; Kim, Y. H.; Wolf, C.; Lee, C. L.; Heo, J. H.; Sadhanala, A.; Myoung, N.; Yoo, S.; Im, S. H.; Friend, R. H.; Lee, T. W. Overcoming The Electroluminescence Efficiency Limitations of Perovskite Light-Emitting Diodes. *Science* **2015**, *350*, 1222–1225.
- (7) Song, J. Z.; Li, J. H.; Li, X. M.; Xu, L. M.; Dong, Y. H.; Zeng, H. B. Quantum Dot Light-Emitting Diodes Based on Inorganic Perovskite Cesium Lead Halides (CsPbX₃). *Adv. Mater.* **2015**, 27, 7162–7167.
- (8) Wang, J. P.; Wang, N. N.; Jin, Y. Z.; Si, J. J.; Tan, Z. K.; Du, H.; Cheng, L.; Dai, X. L.; Bai, S.; He, H. P.; Ye, Z. Z.; Lai, M. L.; Friend, R. H.; Huang, W. Interfacial Control Toward Efficient and Low-Voltage Perovskite Light-Emitting Diodes. *Adv. Mater.* **2015**, 27, 2311–2316.
- (9) Wang, N.; Cheng, L.; Ge, R.; Zhang, S.; Miao, Y.; Zou, W.; Yi, C.; Sun, Y.; Cao, Y.; Yang, R.; Wei, Y.; Guo, Q.; Ke, Y.; Yu, M.; Jin, Y.; Liu, Y.; Ding, Q.; Di, D.; Yang, L.; Xing, G.; Tian, H.; Jin, C.; Gao, F.; Friend, R. H.; Wang, J.; Huang, W. Perovskite Light-Emitting Diodes Based on Solution-Processed Self-Organized Multiple Quantum Wells. *Nat. Photonics* **2016**, *10*, 699–704.
- (10) Zhang, X. Y.; Lin, H.; Huang, H.; Reckmeier, C.; Zhang, Y.; Choy, W. C. H.; Rogach, A. L. Enhancing the Brightness of Cesium Lead Halide Perovskite Nanocrystal Based Green Light-Emitting Devices through the Interface Engineering with Perfluorinated lonomer. *Nano Lett.* **2016**, *16*, 1415–1420.
- (11) Lee, J.-W.; Choi, Y. J.; Yang, J.-M.; Ham, S.; Jeon, S. K.; Lee, J. Y.; Song, Y.-H.; Ji, E. K.; Yoon, D.-H.; Seo, S.; Shin, H.; Han, G. S.; Jung, H. S.; Kim, D.; Park, N.-G. In-Situ Formed Type I Nanocrystalline Perovskite Film for Highly Efficient Light-Emitting Diode. ACS Nano 2017, 11, 3311–3319.
- (12) Xiao, Z.; Kerner, R. A.; Zhao, L.; Tran, N. L.; Lee, K. M.; Koh, T.-W.; Scholes, G. D.; Rand, B. P. Efficient Perovskite Light-Emitting Diodes Featuring Nanometre-Sized Crystallites. *Nat. Photonics* **2017**, *11*, 108–115.
- (13) Zhang, L.; Yang, X.; Jiang, Q.; Wang, P.; Yin, Z.; Zhang, X.; Tan, H.; Yang, Y.; Wei, M.; Sutherland, B. R.; Sargent, E. H.; You, J. Ultra-Bright and Highly Efficient Inorganic Based Perovskite Light-Emitting Diodes. *Nat. Commun.* **2017**, *8*, 15640.
- (14) Xing, G. C.; Mathews, N.; Lim, S. S.; Yantara, N.; Liu, X. F.; Sabba, D.; Gratzel, M.; Mhaisalkar, S.; Sum, T. C. Low-Temperature Solution-Processed Wavelength-Tunable Perovskites for Lasing. *Nat. Mater.* **2014**, *13*, 476–480.
- (15) Stranks, S. D.; Wood, S. M.; Wojciechowski, K.; Deschler, F.; Saliba, M.; Khandelwal, H.; Patel, J. B.; Elston, S. J.; Herz, L. M.; Johnston, M. B.; Schenning, A. P. H. J.; Debije, M. G.; Riede, M. K.; Morris, S. M.; Snaith, H. J. Enhanced Amplified Spontaneous Emission in Perovskites Using a Flexible Cholesteric Liquid Crystal Reflector. *Nano Lett.* **2015**, *15*, 4935–4941.
- (16) Wang, Y.; Li, X.; Song, J.; Xiao, L.; Zeng, H.; Sun, H. All-Inorganic Colloidal Perovskite Quantum Dots: A New Class of Lasing Materials with Favorable Characteristics. *Adv. Mater.* **2015**, 27, 7101–7108.
- (17) Yakunin, S.; Protesescu, L.; Krieg, F.; Bodnarchuk, M. I.; Nedelcu, G.; Humer, M.; De Luca, G.; Fiebig, M.; Heiss, W.; Kovalenko, M. V. Low-Threshold Amplified Spontaneous Emission

- and Lasing from Colloidal Nanocrystals of Caesium Lead Halide Perovskites. *Nat. Commun.* **2015**, *6*, 8056.
- (18) Fu, Y.; Zhu, H.; Stoumpos, C. C.; Ding, Q.; Wang, J.; Kanatzidis, M. G.; Zhu, X.; Jin, S. Broad Wavelength Tunable Robust Lasing from Single-Crystal Nanowires of Cesium Lead Halide Perovskites (CsPbX₃X = Cl, Br, I). ACS Nano **2016**, 10, 7963–7972.
- (19) Xu, Y.; Chen, Q.; Zhang, C.; Wang, R.; Wu, H.; Zhang, X.; Xing, G.; Yu, W. W.; Wang, X.; Zhang, Y.; Xiao, M. Two-Photon-Pumped Perovskite Semiconductor Nanocrystal Lasers. *J. Am. Chem. Soc.* **2016**, *138*, 3761–3768.
- (20) Zheng, F.; Tan, L. Z.; Liu, S.; Rappe, A. M. Rashba Spin—Orbit Coupling Enhanced Carrier Lifetime in CH₃NH₃PbI₃. *Nano Lett.* **2015**, *15*, 7794—7800.
- (21) Hutter, E. M.; Gelvez-Rueda, M. C.; Osherov, A.; Bulovic, V.; Grozema, F. C.; Stranks, S. D.; Savenije, T. J. Direct-Indirect Character of The Bandgap in Methylammonium Lead Iodide Perovskite. *Nat. Mater.* **2017**, *16*, 115–120.
- (22) Tang, B.; Dong, H.; Sun, L.; Zheng, W.; Wang, Q.; Sun, F.; Jiang, X.; Pan, A.; Zhang, L. Single-Mode Lasers Based on Cesium Lead Halide Perovskite Submicron Spheres. *ACS Nano* **2017**, *11*, 10681–10688.
- (23) Deschler, F.; Price, M.; Pathak, S.; Klintberg, L. E.; Jarausch, D.-D.; Higler, R.; Hüttner, S.; Leijtens, T.; Stranks, S. D.; Snaith, H. J.; Atatüre, M.; Phillips, R. T.; Friend, R. H. High Photoluminescence Efficiency and Optically Pumped Lasing in Solution-Processed Mixed Halide Perovskite Semiconductors. *J. Phys. Chem. Lett.* **2014**, *5*, 1421–1426.
- (24) Zhu, H.; Fu, Y.; Meng, F.; Wu, X.; Gong, Z.; Ding, Q.; Gustafsson, M. V.; Trinh, M. T.; Jin, S.; Zhu, X. Y. Lead Halide Perovskite Nanowire Lasers with Low Lasing Thresholds and High Quality Factors. *Nat. Mater.* 2015, 14, 636–642.
- (25) Fu, Y.; Zhu, H.; Schrader, A. W.; Liang, D.; Ding, Q.; Joshi, P.; Hwang, L.; Zhu, X. Y.; Jin, S. Nanowire Lasers of Formamidinium Lead Halide Perovskites and Their Stabilized Alloys with Improved Stability. *Nano Lett.* **2016**, *16*, 1000–1008.
- (26) Zhang, N.; Wang, K.; Wei, H.; Gu, Z.; Sun, W.; Li, J.; Xiao, S.; Song, Q. Postsynthetic and Selective Control of Lead Halide Perovskite Microlasers. *J. Phys. Chem. Lett.* **2016**, *7*, 3886–3891.
- (27) Liu, P.; He, X.; Ren, J.; Liao, Q.; Yao, J.; Fu, H. Organic—Inorganic Hybrid Perovskite Nanowire Laser Arrays. *ACS Nano* **2017**, *11*, *5766*–*5773*.
- (28) Green, M. A.; Emery, K.; Hishikawa, Y.; Warta, W. Solar Cell Efficiency Tables (Version 37). *Prog. Photovoltaics* **2011**, *19*, 84–92.
- (29) Correa-Baena, J.-P.; Saliba, M.; Buonassisi, T.; Grätzel, M.; Abate, A.; Tress, W.; Hagfeldt, A. Promises and Challenges of Perovskite Solar Cells. *Science* **2017**, 358, 739–744.
- (30) Park, N.-G. Organometal Perovskite Light Absorbers Toward a 20% Efficiency Low-Cost Solid-State Mesoscopic Solar Cell. *J. Phys. Chem. Lett.* **2013**, *4*, 2423–2429.
- (31) Yang, W. S.; Noh, J. H.; Jeon, N. J.; Kim, Y. C.; Ryu, S.; Seo, J.; Seok, S. I. High-Performance Photovoltaic Perovskite Layers Fabricated Through Intramolecular Exchange. *Science* **2015**, *348*, 1234–1237.
- (32) Anaraki, E. H.; Kermanpur, A.; Steier, L.; Domanski, K.; Matsui, T.; Tress, W.; Saliba, M.; Abate, A.; Gratzel, M.; Hagfeldt, A.; Correa-Baena, J. P. Highly Efficient and Stable Planar Perovskite Solar Cells by Solution-Processed Tin Oxide. *Energy Environ. Sci.* **2016**, *9*, 3128–3134.
- (33) Bi, D. Q.; Tress, W.; Dar, M. I.; Gao, P.; Luo, J. S.; Renevier, C.; Schenk, K.; Abate, A.; Giordano, F.; Baena, J. P. C.; Decoppet, J. D.; Zakeeruddin, S. M.; Nazeeruddin, M. K.; Gratzel, M.; Hagfeldt, A. Efficient Luminescent Solar Cells Based on Tailored Mixed-Cation Perovskites. *Sci. Adv.* **2016**, *2*, e1501170.
- (34) Momblona, C.; Gil-Escrig, L.; Bandiello, E.; Hutter, E. M.; Sessolo, M.; Lederer, K.; Blochwitz-Nimoth, J.; Bolink, H. J. Efficient Vacuum Deposited p-i-n and n-i-p Perovskite Solar Cells Employing Doped Charge Transport Layers. *Energy Environ. Sci.* **2016**, *9*, 3456—3463.

- (35) Saliba, M.; Matsui, T.; Domanski, K.; Seo, J. Y.; Ummadisingu, A.; Zakeeruddin, S. M.; Correa-Baena, J. P.; Tress, W. R.; Abate, A.; Hagfeldt, A.; Gratzel, M. Incorporation of Rubidium Cations Into Perovskite Solar Cells Improves Photovoltaic Performance. *Science* **2016**, 354, 206–209.
- (36) Arora, N.; Dar, M. I.; Hinderhofer, A.; Pellet, N.; Schreiber, F.; Zakeeruddin, S. M.; Grätzel, M. Perovskite Solar Cells with CuSCN Hole Extraction Layers Yield Stabilized Efficiencies Greater Than 20%. *Science* **2017**, 358, 768–771.
- (37) Shin, S. S.; Yeom, E. J.; Yang, W. S.; Hur, S.; Kim, M. G.; Im, J.; Seo, J.; Noh, J. H.; Seok, S. I. Colloidally Prepared La-doped $BaSnO_3$ Electrodes for Efficient, Photostable Perovskite Solar Cells. *Science* **2017**, 356, 167.
- (38) Stolterfoht, M.; Wolff, C. M.; Amir, Y.; Paulke, A.; Perdigon-Toro, L.; Caprioglio, P.; Neher, D. Approaching the Fill Factor Shockley-Queisser Limit in Stable, Dopant-Free Triple Cation Perovskite Solar Cells. *Energy Environ. Sci.* **2017**, *10*, 1530–1539.
- (39) Tan, H. R.; Jain, A.; Voznyy, O.; Lan, X. Z.; de Arquer, F. P. G.; Fan, J. Z.; Quintero-Bermudez, R.; Yuan, M. J.; Zhang, B.; Zhao, Y. C.; Fan, F. J.; Li, P. C.; Quan, L. N.; Zhao, Y. B.; Lu, Z. H.; Yang, Z. Y.; Hoogland, S.; Sargent, E. H. Efficient and Stable Solution-Processed Planar Perovskite Solar Cells via Contact Passivation. *Science* 2017, 355, 722–726.
- (40) Yang, W. S.; Park, B. W.; Jung, E. H.; Jeon, N. J.; Kim, Y. C.; Lee, D. U.; Shin, S. S.; Seo, J.; Kim, E. K.; Noh, J. H.; Seok, S. I. Iodide Management in Formamidinium-Lead-Halide-Based Perovskite Layers for Efficient Solar Cells. *Science* **2017**, *356*, 1376–1379.
- (41) Sun, S.; Yuan, D.; Xu, Y.; Wang, A.; Deng, Z. Ligand-Mediated Synthesis of Shape-Controlled Cesium Lead Halide Perovskite Nanocrystals via Reprecipitation Process at Room Temperature. *ACS Nano* **2016**, *10*, 3648–3657.
- (42) Shamsi, J.; Dang, Z.; Bianchini, P.; Canale, C.; Di Stasio, F.; Brescia, R.; Prato, M.; Manna, L. Colloidal Synthesis of Quantum Confined Single Crystal CsPbBr₃ Nanosheets with Lateral Size Control up to the Micrometer Range. *J. Am. Chem. Soc.* **2016**, *138*, 7240–7243.
- (43) Akkerman, Q. A.; Motti, S. G.; Srimath Kandada, A. R.; Mosconi, E.; D'Innocenzo, V.; Bertoni, G.; Marras, S.; Kamino, B. A.; Miranda, L.; De Angelis, F.; Petrozza, A.; Prato, M.; Manna, L. Solution Synthesis Approach to Colloidal Cesium Lead Halide Perovskite Nanoplatelets with Monolayer-Level Thickness Control. J. Am. Chem. Soc. 2016, 138, 1010–1016.
- (44) Weidman, M. C.; Seitz, M.; Stranks, S. D.; Tisdale, W. A. Highly Tunable Colloidal Perovskite Nanoplatelets through Variable Cation, Metal, and Halide Composition. *ACS Nano* **2016**, *10*, 7830–7839.
- (45) Weidman, M. C.; Goodman, A. J.; Tisdale, W. A. Colloidal Halide Perovskite Nanoplatelets: An Exciting New Class of Semiconductor Nanomaterials. *Chem. Mater.* **2017**, *29*, 5019–5030.
- (46) Li, J.; Luo, L.; Huang, H.; Ma, C.; Ye, Z.; Zeng, J.; He, H. 2D Behaviors of Excitons in Cesium Lead Halide Perovskite Nanoplatelets. *J. Phys. Chem. Lett.* **2017**, *8*, 1161–1168.
- (47) Protesescu, L.; Yakunin, S.; Bodnarchuk, M. I.; Krieg, F.; Caputo, R.; Hendon, C. H.; Yang, R. X.; Walsh, A.; Kovalenko, M. V. Nanocrystals of Cesium Lead Halide Perovskites (CsPbX3, X = Cl, Br, and I): Novel Optoelectronic Materials Showing Bright Emission with Wide Color Gamut. *Nano Lett.* **2015**, *15*, 3692–3696.
- (48) Makarov, N. S.; Guo, S.; Isaienko, O.; Liu, W.; Robel, I.; Klimov, V. I. Spectral and Dynamical Properties of Single Excitons, Biexcitons, and Trions in Cesium—Lead-Halide Perovskite Quantum Dots. *Nano Lett.* **2016**, *16*, 2349—2362.
- (49) De Roo, J.; Ibáñez, M.; Geiregat, P.; Nedelcu, G.; Walravens, W.; Maes, J.; Martins, J. C.; Van Driessche, I.; Kovalenko, M. V.; Hens, Z. Highly Dynamic Ligand Binding and Light Absorption Coefficient of Cesium Lead Bromide Perovskite Nanocrystals. *ACS Nano* **2016**, *10*, 2071–2081.
- (50) Li, Q.; Zhao, F.; Qu, C.; Shang, Q.; Xu, Z.; Yu, L.; McBride, J. R.; Lian, T. Two-Dimensional Morphology Enhances Light-Driven

- H₂ Generation Efficiency in CdS Nanoplatelet-Pt Heterostructures. *J. Am. Chem. Soc.* **2018**, *140*, 11726–11734.
- (51) Li, Q.; Lian, T. Exciton Dissociation Dynamics and Light-Driven H₂ Generation in Colloidal 2D Cadmium Chalcogenide Nanoplatelet Heterostructures. *Nano Res.* **2018**, *11*, 3031.
- (52) Zhukovskyi, M.; Tongying, P.; Yashan, H.; Wang, Y.; Kuno, M. Efficient Photocatalytic Hydrogen Generation from Ni Nanoparticle Decorated CdS Nanosheets. *ACS Catal.* **2015**, *5*, 6615–6623.
- (53) Zhang, Q.; Chu, L.; Zhou, F.; Ji, W.; Eda, G. Excitonic Properties of Chemically Synthesized 2D Organic—Inorganic Hybrid Perovskite Nanosheets. *Adv. Mater.* **2018**, *30*, 1704055.
- (54) Schnabel, R. F.; Zimmermann, R.; Bimberg, D.; Nickel, H.; Losch, R.; Schlapp, W. Influence of Exciton Localization on Recombination Line-Shapes In_xGa_{1-x}As/GaAs Quantum-Wells as a Model. *Phys. Rev. B: Condens. Matter Mater. Phys.* **1992**, 46, 9873–9876.
- (55) Grim, J. Q.; Christodoulou, S.; Di Stasio, F.; Krahne, R.; Cingolani, R.; Manna, L.; Moreels, I. Continuous-Wave Biexciton Lasing at Room Temperature Using Solution-Processed Quantum Wells. *Nat. Nanotechnol.* **2014**, *9*, 891–895.
- (56) Leosson, K.; Jensen, J. R.; Langbein, W.; Hvam, J. M. Exciton Localization and Interface Roughness in Growth-Interrupted GaAs/AlAs Quantum Wells. *Phys. Rev. B: Condens. Matter Mater. Phys.* **2000**, *61*, 10322–10329.
- (57) Li, Q.; Lian, T. Area- and Thickness-Dependent Biexciton Auger Recombination in Colloidal CdSe Nanoplatelets: Breaking the "Universal Volume Scaling Law. *Nano Lett.* **2017**, *17*, 3152–3158.
- (58) Wu, K.; Liang, G.; Shang, Q.; Ren, Y.; Kong, D.; Lian, T. Ultrafast Interfacial Electron and Hole Transfer from CsPbBr₃ Perovskite Quantum Dots. *J. Am. Chem. Soc.* **2015**, *137*, 12792–12795.
- (59) Yang, Y.; Ostrowski, D. P.; France, R. M.; Zhu, K.; van de Lagemaat, J.; Luther, J. M.; Beard, M. C. Observation of a Hot-Phonon Bottleneck in Lead-Iodide Perovskites. *Nat. Photonics* **2016**, *10*, 53–59.
- (60) Zhao, X.; Kitagawa, T. Solvent Effects of 1,4-Benzoquinone and Its Anion Radicals Probed by Resonance Raman and Absorption Spectra and Their Correlation with Redox Potentials. *J. Raman Spectrosc.* **1998**, *29*, 773–780.
- (61) Huang, J. E.; Huang, Z. Q.; Jin, S. Y.; Lian, T. Q. Exciton Dissociation in CdSe Quantum Dots by Hole Transfer to Phenothiazine. *J. Phys. Chem. C* 2008, 112, 19734–19738.
- (62) Zhu, H. M.; Song, N. H.; Rodriguez-Cordoba, W.; Lian, T. Q. Wave Function Engineering for Efficient Extraction of up to Nineteen Electrons from One CdSe/CdS Quasi-Type II Quantum Dot. *J. Am. Chem. Soc.* **2012**, *134*, 4250–4257.
- (63) Wu, K. F.; Zhu, H. M.; Liu, Z.; Rodriguez-Cordoba, W.; Lian, T. Q. Ultrafast Charge Separation and Long-Lived Charge Separated State in Photocatalytic CdS-Pt Nanorod Heterostructures. *J. Am. Chem. Soc.* **2012**, *134*, 10337–10340.
- (64) Wu, K.; Li, Q.; Du, Y.; Chen, Z.; Lian, T. Ultrafast Exciton Quenching by Energy and Electron Transfer in Colloidal CdSe Nanosheet-Pt Heterostructures. *Chemical Science* **2015**, *6*, 1049–1054.
- (65) Chernikov, A.; Ruppert, C.; Hill, H. M.; Rigosi, A. F.; Heinz, T. F. Population Inversion and Giant Bandgap Renormalization in Atomically Thin WS₂ Layers. *Nat. Photonics* **2015**, *9*, 466–470.
- (66) Klimov, V.; Hunsche, S.; Kurz, H. Biexciton Effects in Femtosecond Nonlinear Transmission of Semiconductor Quantum Dots. *Phys. Rev. B: Condens. Matter Mater. Phys.* **1994**, *50*, 8110–8113.
- (67) Hu, Y. Z.; Koch, S. W.; Lindberg, M.; Peyghambarian, N.; Pollock, E. L.; Abraham, F. F. Biexcitons in Semiconductor Quantum Dots. *Phys. Rev. Lett.* **1990**, *64*, 1805–1807.
- (68) Hintermayr, V. A.; Polavarapu, L.; Urban, A. S.; Feldmann, J. Accelerated Carrier Relaxation through Reduced Coulomb Screening in Two-Dimensional Halide Perovskite Nanoplatelets. *ACS Nano* **2018**, *12*, 10151–10158.

- (69) Feldmann, J.; Peter, G.; Göbel, E. O.; Dawson, P.; Moore, K.; Foxon, C.; Elliott, R. J. Linewidth Dependence of Radiative Exciton Lifetimes in Quantum Wells. *Phys. Rev. Lett.* **1987**, *59*, 2337–2340.
- (70) 't Hooft, G. W.; Van der Poel, W. A. J. A.; Molenkamp, L. W.; Foxon, C. T. Giant Oscillator Strength of Free Excitons in GaAs. *Phys. Rev. B: Condens. Matter Mater. Phys.* 1987, 35, 8281–8284.
- (71) Ithurria, S.; Tessier, M. D.; Mahler, B.; Lobo, R. P. S. M.; Dubertret, B.; Efros, A. Colloidal Nanoplatelets with Two-Dimensional Electronic Structure. *Nat. Mater.* **2011**, *10*, 936–941.
- (72) Klimov, V.; Bolivar, P. H.; Kurz, H. Ultrafast Carrier Dynamics in Semiconductor Quantum Dots. *Phys. Rev. B: Condens. Matter Mater. Phys.* **1996**, *53*, 1463–1467.
- (73) Hunsche, S.; Dekorsy, T.; Klimov, V.; Kurz, H. Ultrafast Dynamics of Carrier-Induced Absorption Changes in Highly-Excited CdSe Nanocrystals. *Appl. Phys. B: Lasers Opt.* **1996**, *62*, 3–10.
- (74) Klimov, V. I.; Schwarz, C. J.; McBranch, D. W.; Leatherdale, C. A.; Bawendi, M. G. Ultrafast Dynamics of Inter- and Intraband Transitions in Semiconductor Nanocrystals: Implications for Quantum-Dot Lasers. *Phys. Rev. B: Condens. Matter Mater. Phys.* 1999, 60, R2177–R2180.
- (75) Klimov, V. I. Optical Nonlinearities and Ultrafast Carrier Dynamics in Semiconductor Nanocrystals. *J. Phys. Chem. B* **2000**, *104*, 6112–6123.
- (76) Wu, K.; Lian, T. Quantum Confined Colloidal Nanorod Heterostructures for Solar-to-Fuel Conversion. *Chem. Soc. Rev.* **2016**, 45, 3781–3810.
- (77) Wu, K.; Zhu, H.; Lian, T. Ultrafast Exciton Dynamics and Light-Driven H₂ Evolution in Colloidal Semiconductor Nanorods and Pt-Tipped Nanorods. *Acc. Chem. Res.* **2015**, *48*, 851–859.
- (78) Wu, K. F.; Rodriguez-Cordoba, W. E.; Liu, Z.; Zhu, H. M.; Lian, T. Q. Beyond Band Alignment: Hole Localization Driven Formation of Three Spatially Separated Long-Lived Exciton States in CdSe/CdS Nanorods. *ACS Nano* **2013**, *7*, 7173–7185.
- (79) Wu, K.; Li, Q.; Jia, Y.; McBride, J. R.; Xie, Z.-x.; Lian, T. Efficient and Ultrafast Formation of Long-Lived Charge-Transfer Exciton State in Atomically Thin Cadmium Selenide/Cadmium Telluride Type-II Heteronanosheets. ACS Nano 2015, 9, 961–968.
- (80) Li, Q.; Xu, Z.; McBride, J. R.; Lian, T. Low Threshold Multiexciton Optical Gain in Colloidal CdSe/CdTe Core/Crown Type-II Nanoplatelet Heterostructures. *ACS Nano* **2017**, *11*, 2545–2553.
- (81) Li, Q.; Zhou, B.; McBride, J. R.; Lian, T. Efficient Diffusive Transport of Hot and Cold Excitons in Colloidal Type II CdSe/CdTe Core/Crown Nanoplatelet Heterostructures. *ACS Energy Letters* **2017**, 2, 174–181.
- (82) Li, Q.; Wu, K.; Chen, J.; Chen, Z.; McBride, J. R.; Lian, T. Size-Independent Exciton Localization Efficiency in Colloidal CdSe/CdS Core/Crown Nanosheet Type-I Heterostructures. *ACS Nano* **2016**, 10, 3843–3851.
- (83) Morris-Cohen, A. J.; Frederick, M. T.; Cass, L. C.; Weiss, E. A. Simultaneous Determination of the Adsorption Constant and the Photoinduced Electron Transfer Rate for a Cds Quantum Dot–Viologen Complex. *J. Am. Chem. Soc.* **2011**, *133*, 10146–10154.
- (84) Wu, K.; Du, Y.; Tang, H.; Chen, Z.; Lian, T. Efficient Extraction of Trapped Holes from Colloidal CdS Nanorods. *J. Am. Chem. Soc.* **2015**, 137, 10224–10230.
- (85) Song, N. H.; Zhu, H. M.; Jin, S. Y.; Lian, T. Q. Hole Transfer from Single Quantum Dots. *ACS Nano* **2011**, *5*, 8750–8759.
- (86) Song, N. H.; Zhu, H. M.; Jin, S. Y.; Zhan, W.; Lian, T. Q. Poisson-Distributed Electron-Transfer Dynamics from Single Quantum Dots to C₆₀ Molecules. *ACS Nano* **2011**, *5*, 613–621.
- (87) Zhu, H. M.; Lian, T. Q. Enhanced Multiple Exciton Dissociation from CdSe Quantum Rods: The Effect of Nanocrystal Shape. *J. Am. Chem. Soc.* **2012**, *134*, 11289–11297.
- (88) Zhu, H. M.; Lian, T. Q. Wavefunction Engineering in Quantum Confined Semiconductor Nanoheterostructures for Efficient Charge Separation and Solar Energy Conversion. *Energy Environ. Sci.* **2012**, *5*, 9406–9418.

- (89) Wu, K. F.; Song, N. H.; Liu, Z.; Zhu, H. M.; Rodriguez-Cordoba, W.; Lian, T. Q. Interfacial Charge Separation and Recombination in InP and Quasi-Type II InP/CdS Core/Shell Quantum Dot-Molecular Acceptor Complexes. *J. Phys. Chem. A* **2013**, *117*, 7561–7570.
- (90) Zhu, H.; Yang, Y.; Hyeon-Deuk, K.; Califano, M.; Song, N.; Wang, Y.; Zhang, W.; Prezhdo, O. V.; Lian, T. Auger-Assisted Electron Transfer from Photoexcited Semiconductor Quantum Dots. *Nano Lett.* **2014**, *14*, 1263–1269.
- (91) Zhu, H. M.; Yang, Y.; Lian, T. Q. Multiexciton Annihilation and Dissociation in Quantum Confined Semiconductor Nanocrystals. *Acc. Chem. Res.* **2013**, *46*, 1270–1279.
- (92) Congreve, D. N.; Weidman, M. C.; Seitz, M.; Paritmongkol, W.; Dahod, N. S.; Tisdale, W. A. Tunable Light-Emitting Diodes Utilizing Quantum-Confined Layered Perovskite Emitters. *ACS Photonics* **2017**, *4*, 476–481.
- (93) Tsai, H.; Nie, W.; Blancon, J.-C.; Stoumpos, C. C.; Asadpour, R.; Harutyunyan, B.; Neukirch, A. J.; Verduzco, R.; Crochet, J. J.; Tretiak, S.; Pedesseau, L.; Even, J.; Alam, M. A.; Gupta, G.; Lou, J.; Ajayan, P. M.; Bedzyk, M. J.; Kanatzidis, M. G.; Mohite, A. D. High-Efficiency Two-Dimensional Ruddlesden—Popper Perovskite Solar Cells. *Nature* **2016**, *536*, 312—316.